NEW RESULTS FROM HERMES

M. TYTGAT*

University of Gent,
Dept. Subatomic and Radiation Physics,
Proeftuinstraat 86,
9000 Gent, Belgium
E-mail: michael@inwfsun1.UGent.be

An overview is given of selected recent HERMES results obtained from measurements performed during the first running period of HERA. These topics include inclusive $g_1(x)$-measurements with a NLO QCD analysis, polarized quark distribution extraction, $b_1(x)$-measurement, double spin asymmetries in vector meson production, ρ^0-nuclear transparency and finally quark fragmentation in nuclei.

1. Introduction

The HERMES experiment uses the 27.5 GeV polarized HERA electron/positron beam to scatter deep-inelastically off a (un)polarized fixed gaseous nuclear target. Data taking began in 1995, during the first HERA running period and still continues with HERA-II. Although HERMES was originally designed to study the nucleon spin in polarized DIS, a wide range of physics topics has been addressed over the past years. Here only some of the recent results from HERA-I will be summarized. First results obtained during HERA-II are discussed elsewhere [1].

2. NLO QCD Analysis of the $g_1(x, Q^2)$ Structure Function

During HERA-I HERMES performed longitudinally polarized inclusive DIS measurements on ^{1}H, ^{2}H and ^{3}He. A compilation of the world data on the $g_1(x, Q^2)$-structure function including the HERMES results is displayed in figure 1. The HERMES data actually add most precision to g_1^d. Considering $g_1 = \frac{1}{2}\sum_q e_q^2 \Delta q$ in the naïve parton model with Δq being the polarized quark densities and neglecting the quark sea, one can qualitatively deduce

*On behalf of the HERMES Collaboration

from these inclusive data that Δu must be large and positive, while Δd should be negative.

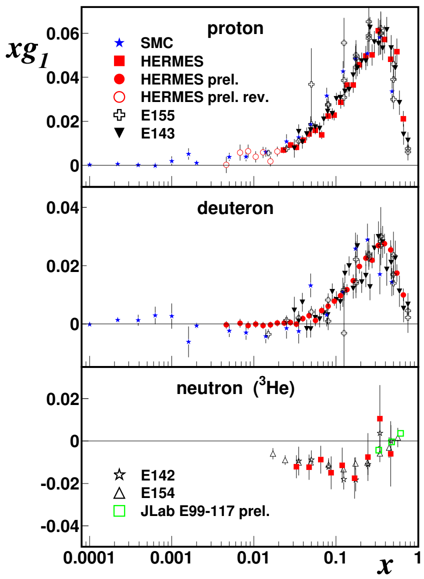

Figure 1. A compilation of recent world data on $xg_1(x, Q^2)$ for the proton, deuteron and neutron.

To obtain more quantitative information on the polarized quark densities a next-to-leading order QCD analysis of the $g_1(x, Q^2)$-data was carried out including the latest HERMES results. The $g_1(x, Q^2)$-structure function was parametrized as a Mellin convolution in terms of the polarized singlet density $\Delta\Sigma = \sum_{i=1}^{N_f}[\Delta q_i + \Delta\bar{q}_i]$, the polarized gluon density ΔG and the polarized non-singlet densities $\Delta q_i^{NS} = \Delta q_i + \Delta\bar{q}_i - 1/N_f \cdot \Delta\Sigma$. In the evolution equations the polarized splitting functions and Wilson coefficient functions are calculated in NLO in the $\overline{\mathrm{MS}}$-scheme. Two independent methods were used to extract the parton densities. The first one is a numerical method with evolution in x-space and takes $\Delta\Sigma$, Δq_p^{NS}, Δq_n^{NS} and ΔG as distributions to be determined in the fit. The second method solves the evolution equations in Mellin-N space and uses Δu_v, Δd_v, $\Delta\bar{q}_s$ and ΔG as free distributions. The polarized parton densities at input scale $Q_0^2 = 4.0$ GeV^2 were parametrized in the form $x\Delta q_i(x, Q_0^2) = \eta_i A_i x^{a_i}(1-x)^{b_i}(1 + \gamma_i x + \rho_i x^{1/2})$, where the normalization constants A_i are chozen such that η_i represents the first moment of Δq_i.

Both method produce compatible results and the final polarized parton densities as determined with the second method are displayed in figure 2 at input scale, where they are compared to previous analyses [2,3]. The shaded

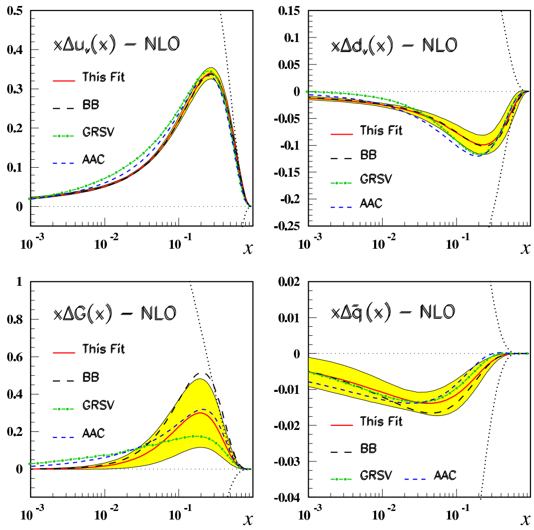

Figure 2. The polarized quark distributions at $Q_0^2 = 4.0$ GeV^2 compared to previous analyses. The dark dotted lines correspond to the positivity limits from unpolarized distributions.

areas denote the fully correlated 1σ statistical error bands and the dotted lines correspond to the positivity limits from unpolarized distributions. While Δu_v and Δd_v are well constrained by the current fit, ΔG and $\Delta\bar{q}$ remain poorly determined. For ΔG the theoretical uncertainty dominates the overal systematic error, such that not only an improved data set with a larger Q^2-range but also a NNLO calculation could improve the situation.

3. Flavor Decomposition of Polarized Quark Distributions

Another method to accomplish a flavor decomposition of the polarized quark densities is provided by flavor tagging in polarized semi-inclusive DIS [4] $e + p(d) \to e + h + X$. The measured photon-nucleon double spin asymmetry A_1^h for semi-inclusive events with a leading hadron of type h

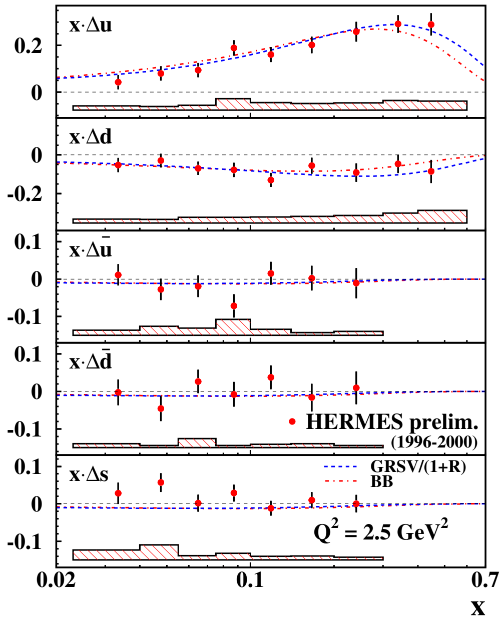

Figure 3. The polarized parton densities at $Q^2 = 2.5$ GeV^2.

can be written as

$$A_1^h(x, Q^2) \sim \sum_q \frac{e_q^2 q(x, Q^2) \int \mathrm{d}z D_q^h(z, Q^2)}{\sum_{q'} e_{q'}^2 q'(x, Q^2) \int \mathrm{d}z D_{q'}^h(z, Q^2)} \frac{\Delta q}{q}(x, Q^2) \tag{1}$$

$$\sim \sum_q P_q^h(x, Q^2) \frac{\Delta q}{q}(x, Q^2), \tag{2}$$

with D_q^h being the fragmentation function for a quark flavor q and Δq (q) being the (un)polarized quark density. The purity P_q^h represents the probability that the hadron h originates from an event in which a quark of flavor q was struck by the virtual photon. The purities are spin-independent quantities and were evaluated using the PEPSI/JETSET DIS Monte Carlo model [5]. The CTEQ5L parametrizations for unpolarized quark densities were used and the JETSET fragmentation parameters were tuned to reproduce the hadron multiplicities measured at HERMES. Equation 2 can be rewritten as a matrix equation $\vec{A} = P \cdot \vec{Q}$, where $\vec{A} = (A_{1p}, A_{1p}^{\pi^\pm}, A_{1d}, A_{1d}^{\pi^\pm}, A_{1d}^{K^\pm})$ contains the measured inclusive and semi-inclusive asymmetries on the proton and deuteron, P contains the purities for the proton and deuteron and $\vec{Q} = (\frac{\Delta u}{u}, \frac{\Delta d}{d}, \frac{\Delta \bar{u}}{\bar{u}}, \frac{\Delta \bar{d}}{\bar{d}}, \frac{\Delta s}{s}, \frac{\Delta \bar{s}}{\bar{s}})$ contains the quark and anti-quark polarizations to be determined. The matrix equation was solved by χ^2-minimization and the resulting polarized parton densities are depicted in figure 3 at the mean scale $< Q^2 >= 2.5$ GeV^2. While Δu is positive in the measured x-range, Δd appears negative and only slightly dependent on x. Both distributions are consistent with previous measurements, but are now known with a much improved precision. The light sea quark polarization densities are compatible with zero. The densities in the figure are compared to two leading order QCD fits [2].

4. The $b_1(x, Q^2)$ Tensor Structure Function

When scattering off a spin-1 target an additional leading twist structure function $b_1(x, Q^2)$ enters the symmetric part of the hadronic tensor compared to the spin-1/2 case. This structure function measures the difference in the polarized quark distributions of a target with helicity $m = \pm 1$ and $m = 0$: $b_1(x, Q^2) = \frac{1}{2}\sum_i e_i^2[2q_i^0(x, Q^2) - q_i^+(x, Q^2) - q_i^-(x, Q^2)]$. The cross section now depends on the vector and tensor polarization of the target $\sigma = \sigma_u[1 + P_b\ V\ A_\parallel + \frac{1}{2}\ T\ A_T]$, where $A_\parallel \sim g_1/F_1$ and $A_T \sim -2/3 \cdot b_1/F_1$ are the target vector and tensor asymmetry respectively, V and T the target vector and tensor polarization and P_b the beam polarization.

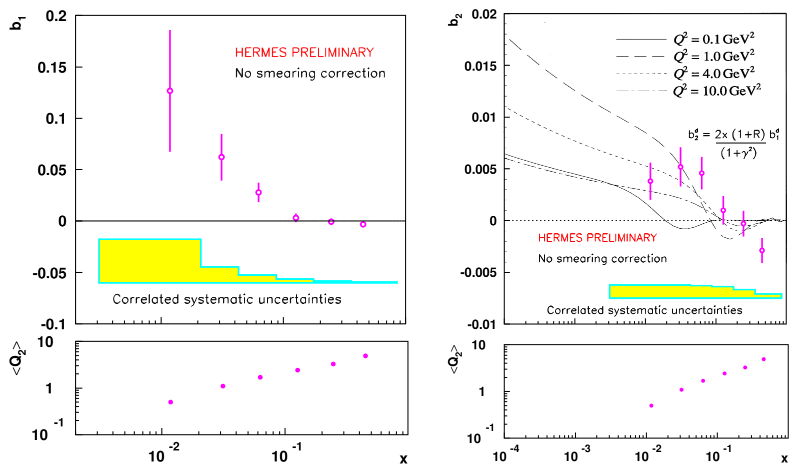

Figure 4. The measured $b_1(x, Q^2)$ and $b_2(x, Q^2)$ structure function on the deuteron.

The tensor asymmetry A_T was measured for the first time at HERMES on the deuteron target in the kinematic range $0.0021 < x < 0.85$ and

$0.1 < Q^2 < 20$ GeV^2. The resulting b_1 is shown in figure 4 together with b_2, which is related to the former via a Callan-Gross like relation. At small x both structure functions appear positive which can be interprated as being due to the quadrupole deformation of the deuteron. The b_2-data is in qualitative agreement with the double scattering model calculations from Ref. 6.

5. Double-Spin Asymmetries in Vector Meson Production

The longitudinally polarized beam and target allows HERMES to investigate double-spin asymmetries in vector meson production [7]. Averaged over the kinematic acceptance the asymmetries for exclusive ρ^0-production were found to be $0.23 \pm 0.14 \pm 0.02$ on the proton and $-0.040 \pm 0.076 \pm 0.013$ on the deuteron for average kinematics $< W >= 4.9$ GeV, $< Q^2 >= 1.8$ GeV^2 and $< -t' >= 0.15$ GeV^2. The same asymmetries extracted for the ϕ-meson were compatible with zero. Figure 5 displays the ρ^0 asymmetries for both targets as function of Bjorken x and Q^2. Using the HERMES data

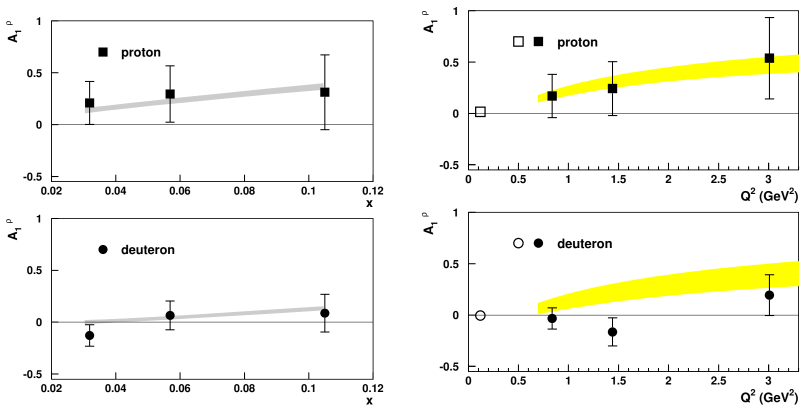

Figure 5. Double-spin asymmetry in ρ^0-production from a polarized hydrogen and deuterium target as function of Bjorken x and Q^2.

on A_1^N and the simple relation $A_1^\rho = 2A_1^N/(1 + (A_1^N)^2)$ between the vector meson and inclusive DIS asymmetry as derived in Ref. 8, one obtains the shaded bands in figure 5 for the x-dependence of the asymmetries. Both the proton and deuteron asymmetries are consistent with this prediction. The Q^2-dependences are compared to a Regge model calculation from Ref. 9. In this model the parameters of the Reggeons contributing to ρ^0-production were extracted from fits to g_1^N and F_2^N. While the proton measurement seems to agree with the prediction, the deuteron data lies below the calculation. The datapoints at the lowest Q^2-value are both compatible with zero and were obtained with a special trigger for events in wich the beam particle scatters at too low angles to be detected.

In Ref. 8 the non-zero asymmetry result for ρ^0-production arises from an interference between natural and unnatural parity exchange amplitudes. Since the Pomeron has natural parity, it is suggested that at HERMES energies the transverse ρ^0-production amplitude on the proton receives significant contributions from Reggeon or di-quark exchange. This not only agrees with the previous observation that at HERMES the longitudinal production amplitude on the proton is dominated by quark exchange [10], but also is not in contradiction with the vanishing asymmetry found at higher energies at SMC [11], where ρ^0-production is dominated by gluon exchange and also the inclusive asymmetry is much smaller. The zero asymmetry result for ϕ-production, which is dominated by Pomeron exchange even at HERMES energies, can also be understood in the same way.

6. Color Transparency in ρ^0-Production

A fundamental prediction of QCD is the existence of the color transparency (CT) phenomenon, i.e. a hadron which is produced at sufficiently high Q^2 will traverse a nuclear medium with vanishing initial and final state interactions. In the search for CT one commonly uses the nuclear transparency $T = \sigma_A/(A\sigma_p)$, which is the ratio of the nuclear cross section per nucleon to the one on the proton. The distance which the $q\bar{q}$-fluctuation of the virtual photon in ρ^0-production can propagate is the coherence length $l_c = 2\nu/(Q^2 + M_{q\bar{q}}^2)$. This latter quantity is important for CT-studies, especially for incoherent ρ^0-production, where at l_c-values smaller than the nuclear size T increases with Q^2 due to the coherence length effect previously observed at HERMES [12]. For coherent ρ^0-production the drop of the nuclear form factor at high Q^2 (small l_c) causes a decreasing behavior of T with Q^2. In order to get a clean signature of a CT-effect, one has to disentangle the coherence length effects from those of CT, which can be done by studying T as function of Q^2 for fixed l_c [13]. Figure 6 shows the measured T for both coherent and incoherent exclusive ρ^0-production on nitrogen as function of Q^2 for small intervals of l_c [14]. The data were fitted with a common Q^2-slope equal to 0.074 ± 0.023 GeV^{-2}, which agrees with the theoretical prediction of about 0.058 GeV^{-2}. This positive slope of the

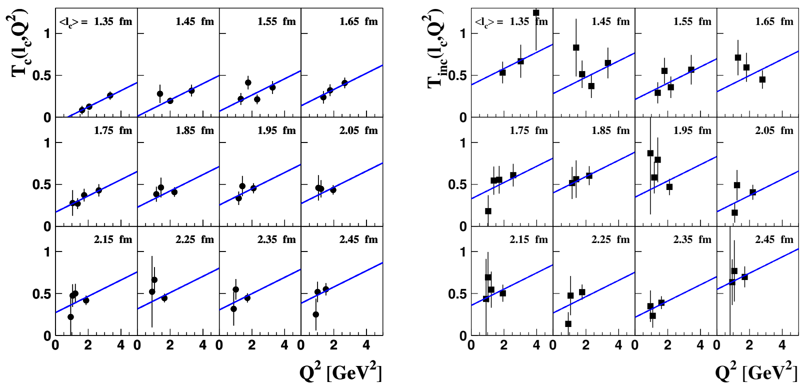

Figure 6. The left (right) plot shows the nuclear transparency for (in)coherent ρ^0-production on nitrogen as function of Q^2 for several coherence lenght intervals.

Q^2-dependence represents a signature of color transparency.

7. Quark Fragmentation in Nuclei

In deep-inelastic scattering off a nucleus, the nuclear medium acts as an ensemble of targets for the quark struck by the virtual photon and for the produced hadrons and will therefore influence the hadronization process. Due to multiple interactions with the surrounding medium and induced gluon radiation the struck quark will lose energy. A final hadron formed inside the nucleus can also interact via the hadronic interaction cross section with the nuclear medium. Both effects will induce a softening of the leading hadron spectra compared to the free nucleon case. The hadronization process in nuclear media is usually described either in phenomenological string models including final state interactions of the produced hadron or in more QCD-inspired models by e.g. parton energy loss or gluon-bremsstrahlung. A clean tool to study nuclear effects in quark propagation and hadronization is semi-inclusive DIS, where one usually examines the multiplicity ratio for a hadron h on a nucleus A compared to the deuteron,

$$R^h_M(z,\nu,p_t^2,Q^2) = \frac{(N_h(z,\nu,p_t^2,Q^2)/N_e(\nu,Q^2))\big|_A}{(N_h(z,\nu,p_t^2,Q^2)/N_e(\nu,Q^2))\big|_D}, \qquad (3)$$

with N_h the semi-inclusive yield normalized to the inclusive yield N_e.

The multiplicity ratios for π, K, p and $\bar{p}$ measured by HERMES [15] on ^{84}Kr are displayed in figure 7 as function of ν and z. Contributions due to target fragmentation were suppressed by requiring $z > 0.2$ and large

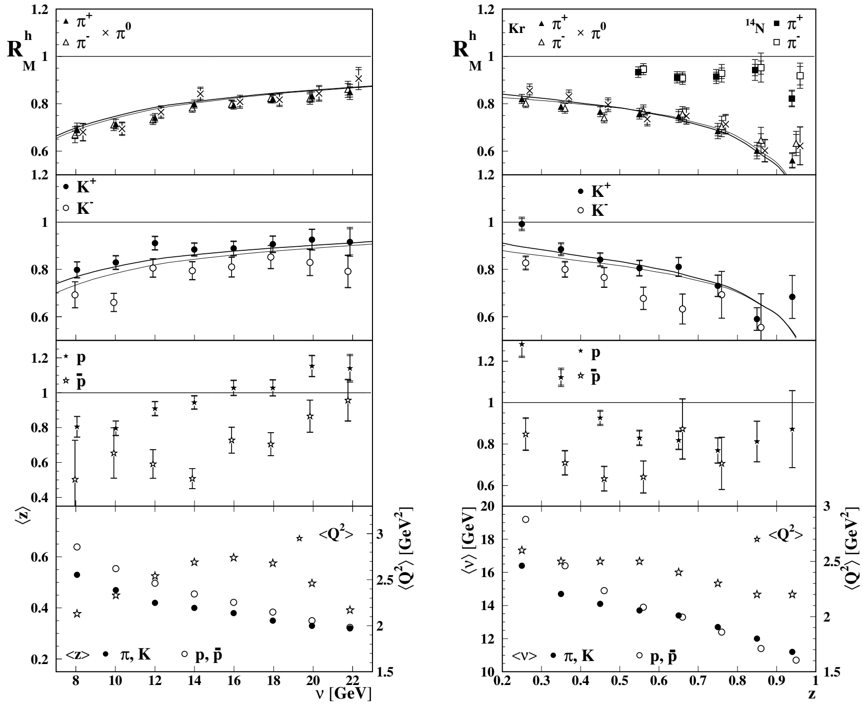

Figure 7. Multiplicity ratios for π, K, p and $\bar{p}$ for ^{84}Kr as function of ν and z. The z-dependence of the π multiplicity on ^{14}N is also shown.

acceptance effects in z were avoided by taking $\nu > 7$ GeV. The plot also includes the π-multiplicity z-dependence on ^{14}N [16]. The multiplicity ratios for π^+, π^- and π^0 on krypton appear to be similar, which is also true for the nitrogen $\pi^{\pm}$-data. Whereas the multiplicity ratio for K^- is compatible with that for pions, the K^+-multiplicity ratio is significantly larger and an even larger difference is observed between p and $\bar{p}$. One way to understand these differences is to interpret them in terms of different hadron formation times for mesons and baryons in combination with different hadron-nucleon interaction cross sections. The curves in the plots represent the result of a model calculation [19] based on a rescaling of the quark fragmentation due to the nuclear medium. In Ref. 17 the differences are attributed to a mixing of quark and gluon fragmentation functions in nuclei due to multiple parton scattering, such that quark and anti-quark fragmentation functions receive different medium modifications. The π-data on both targets exhibit the same trend, however as expected, the attenuation in krypton appears much stronger than in nitrogen. The mass dependence of the nuclear attenuation $1 - R_M^h$ appears closer to a $A^{2/3}$-dependence as predicted in Ref. 17 than to a $A^{1/3}$-dependence suggested by models based on nuclear absorption only.

Another nuclear effect is the Cronin effect [18], which concerns the broadening of the hadron p_t-distribution on a nuclear target compared to the proton due to multiple scattering of the propagating quark and hadron. This phenomenon was also observed by HERMES [15] as an enhancement of the charged hadron multiplicity ratio on ^{14}N and ^{84}Kr at high p_t^2. It is similar to the effect seen in proton-nucleus and nucleus-nucleus collisions and may help to interpret the new heavy-ion data from SPS and RHIC.

Acknowledgments

The author would like to acknowledge the support of the FWO-Flanders, Belgium, for this work.

References

1. E.C. Aschenauer, Plans of the HERMES experiment at HERA-II, same proceedings.
2. J. Blümlein and H. Böttcher, Nucl. Phys. **B636**, 225 (2002); M. Glück *et al.*, Phys. Rev. **D63**, 094005 (2001).
3. Y. Goto *et al.*, Phys. Rev. **D62**, 034017 (2000).
4. A. Airapetian *et al.*, Phys. Rev. Lett (in press), hep-ex/0307064
5. L. Mankiewicz *et al.*, Phys. Comm. **71**, 305 (1992); T. Sjöstrand *et al.*, Comp. Phys. Comm. **135**, 238 (2001).
6. K. Bora and R.L. Jaffe, Phys. Rev. **D57**, 6906 (1998).
7. A. Airapetian *et al.*, Phys. Lett. **B513**, 301 (2001);Eur. Phys. J. **C29**, 171 (2003).
8. H. Fraas, Nucl. Phys. **B113**, 532 (1976).
9. N.I. Kochelev *et al.*, Phys. Rev. **D65**, 097504 (2002); Phys. Rev. **D67**, 074014 (2003)
10. A. Airapetian *et al.*, Eur. Phys. J. **C17**, 389 (2000).
11. A. Tripet for the SMC Collaboration, Nucl. Phys. **B79**, 529 (1999).
12. K. Ackerstaff *et al.*, Phys. Rev. Lett. **82**, 3025 (1999).
13. B.Z. Kopeliovich *et al.*, Phys. Rev. **C65**, 035201 (2002).
14. A. Airapetian *et al.*, Phys. Rev. Lett. **90**, 052501 (2003).
15. A. Airapetian *et al.*, Phys. Lett. B (in press); hep-ex/0307023.
16. A. Airapetian *et al.*, Eur. Phys. J. **C20**, 479 (2001).
17. X.N. Wang and X. Guo, Nucl. Phys. **A696**, 788 (2001); E. Wang and X.N. Wang, Phys. Rev. Lett. **89**, 162301 (2002)
18. J.W. Cronin *et al.*, Phys. Rev. **D11**, 3105 (1975).
19. A. Accardi, V. Muccifora, H.J. Pirner, Nucl. Phys. **A720**, 131 (2003).